Facile synthesis of Prussian blue nanocubes/silver nanowires network as a water-based ink for the direct screen-printed flexible biosensor chips

Pengqi Yang, Jingmeng Peng, Zhenyu Chu, Danfeng Jiang, Wanqin Jin

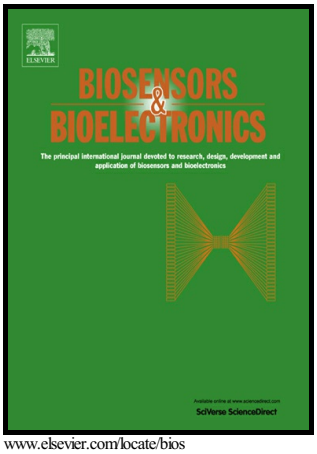

www.elsevier.com/locate/bios

PII: S0956-5663(16)31009-0
DOI: http://dx.doi.org/10.1016/j.bios.2016.10.013
Reference: BIOS9235

To appear in: *Biosensors and Bioelectronic*

Received date: 25 July 2016
Revised date: 20 September 2016
Accepted date: 4 October 2016

Cite this article as: Pengqi Yang, Jingmeng Peng, Zhenyu Chu, Danfeng Jiang and Wanqin Jin, Facile synthesis of Prussian blue nanocubes/silver nanowires network as a water-based ink for the direct screen-printed flexible biosensor chips, *Biosensors and Bioelectronic* http://dx.doi.org/10.1016/j.bios.2016.10.013

Facile synthesis of Prussian blue nanocubes/silver nanowires network as a water-based ink for the direct screen-printed flexible biosensor chips

Pengqi Yang, Jingmeng Peng, Zhenyu Chu, Danfeng Jiang, Wanqin Jin*

State Key Laboratory of Materials-Oriented Chemical Engineering, College of Chemical Engineering, Nanjing Tech University, Nanjing 210009, P. R. China
*Corresponding Author. Tel: +86 25 8317 2266; fax:+86 25 8317 2292. wqjin@njtech.edu.cn

Abstract

The large-scale fabrication of nanocomposite based biosensors is always a challenge in the technology commercialization from laboratory to industry. In order to address this issue, we have designed a facile chemical method of fabricated nanocomposite ink applied to the screen-printed biosensor chip. This ink can be derived in the water through the *in-situ* growth of Prussian blue nanocubes (PBNCs) on the silver nanowires (AgNWs) to construct a composite nanostructure by a facile chemical method. Then a miniature flexible biosensor chip was screen-printed by using the prepared nanocomposite ink. Due to the synergic effects of the large specific surface area, high conductivity and electrocatalytic activity from AgNWs and PBNCs, the as-prepared biosensor chip exhibited a fast response (< 3 s)， a wider linear response from 0.01 mM to 1.3 mM with an ultralow LOD = 5 μM, and the ultrahigh sensitivities of 131.31 and 481.20 μA mM^{-1} cm^{-2} for the detections of glucose and hydrogen peroxide (H_2O_2), respectively. Furthermore, the biosensor chip exhibited excellent

stability, good reproducibility and high anti-interference ability towards physiological substances under a very low working potential of -0.05. Hence, the proposed biosensor chip also showed a promising potential for the application in practical analysis.

Keywords

silver nanowires; Prussian blue nanocubes; screen-printed biosensor chips; high sensitivity

1. Introduction

In recent years, electrochemical biosensors have harvested fast development in the fields of clinical diagnosis, environmental pollution monitor and food quality analysis, in virtue of their practical advantages of operation convenience, low cost and the *in-situ* analysis mode (Lu et al. 2012; Wang et al. 2014; Zhang et al. 2015). However, rare achievements have been developed to the commercial products due to the unsatisfied performance or limits of preparation methods on a large scale. The enzymatic biosensor is one of the most important categories of electrochemical biosensor due to its excellent selectivity from the specificity of enzyme reaction. Clark and Lyon proposed the first generation of the concept of the enzymatic biosensor in 1962, and successfully applied it in the Children's Hospital of Cincinnati (L. C. Clark 1962). The enzymatic biosensor is primarily consisted by three elements: (i) the biological enzyme recognizes the specific molecule; (ii) a transducer film converts the bio-signal into the electric signal; (iii) a signal processing system converts the electric signal into a readable form (L. C. Clark 1962; Wu et al. 2015; Yoo and Lee 2010). The bio-signal is normally generated by the enzyme reaction (Piao et al. 2015).The common enzyme oxidation reaction can produce a by-product of H_2O_2 (Liu et al. 2015). It is in accordance with the reaction as follows (Song et al.

2006; Wang et al. 2013):

$$\text{Substrate} + O_2 \xrightarrow{\text{oxidase}} \text{Product (oxidized substrate)} + H_2O_2 \quad (1)$$

Prussian blue (PB), which is a porous metal coordination complex, is considered as an "artificial peroxidase" (Karyakin and Karyakina 1999; Liu et al. 2009; Liu et al. 2009; Zhang et al. 2011) because of its high electrocatalytic activity to H_2O_2. Accordingly, PB is an excellent film material of signal transducer for the construction of oxidase-based biosensors (Espinoza-Castañeda et al. 2015; Keihan and Sajjadi 2013). The recent research results of PB reveal that the nanostructures can give rise to the catalysis and chemical stability (Xu et al. 2015). However, the conductivity of PB is always an obstacle due to its 1.43 eV band gap (Chu et al. 2010). Especially for the formation of regular nanostructure based film, PB crystal is independent with large gaps during the stacking together, which causes the obvious increase of resistance for signal transfer to heavily decrease the performance. In order to address above issue, a special material with high conductivity is required to introduce for covering this deficiency.

Definitely, there are numerous materials which can promote the electron transfer. However, due to the saturated coordination status of PB with less interaction sites for combination, it is difficult that construct a skeleton to realize the uniform and *in-situ* growth of PB for the regular nanostructure formation. As our previous work (Chu et al. 2009), the noble metal can produce the Van der Waals force for the PB growth although this interaction is weak. Therefore, gold, silver, platinum and etc. can be served as the candidate foundation for PB deposition. Silver nanowires (AgNWs) have been applied in biosensor due to its large surface area and superior conductivity (A. S. Rad et al. 2011; Ren et al. 2005). Moreover, it can knit a three-dimensional (3D) network which possesses the abundant sites for PB growth. Therefore, the composite

of PB and AgNWs can be expected to produce an advanced biosensor with high performance.

In this work, we have designed a novel large-scale synthesis route to realize the *in-situ* growth of PB nanocrystals on the AgNWs 3D skeleton. The PB nanocubes (PBNCs) were uniformly synthetized on the the surface of AgNW by a low-speed chemical synthesis method and the AgNWs network could be remained (Fig. 2C), in which the electrocatalytic activity of PBNCs/AgNWs could be markedly enhanced. Due to the high electrocatalysis and conductivity of the 3D nanocomposite, the as-printed biosensor chip has exhibited the excellent sensitivities to the detections of H_2O_2 and glucose, as well as good selectivity and stability under the very low potential -0.05 V. Meantime, the biosensor chips have a wider range of detection (ROD) and a lower limit of detection (LOD). Therefore, the prepared biosensor chip possesses the promising applications in the recognitions of heavy metal and physiological substances.

2. Experimental

2.1. Reagents and apparatus

All chemicals were of analytical purity and used as received. Potassium ferrocyanide trihydrate ($K_4[Fe(CN)_6]\cdot 3H_2O$), iron(III) chloride hexahydrate ($FeCl_3\cdot 6H_2O$), ethylene glycol (EG) and glucose oxidase (GOx) from Aspergillus niger (E.C.1.1.3.4, 180200 U/g) were purchased from Sigma–Aldrich. Silver nitrate ($AgNO_3$) and polyvinylpyrrolidone (PVP) (Mw ≈ 40,000) were purchased from the Shanghai Chemical Reagent Company. Hydrochloric acid (HCl), potassium chloride (KCl), sodium chloride (NaCl) and glutaraldehyde 25% (v/v) were obtained from Shanghai Lingfeng Chemical Reagent Co. Ltd. (China). Sodium L-lactate and sodium

glutamic acid monosodium salt monohydrate were purchased from Alfa-Aesar. Hydrogen peroxide (H_2O_2, 30%, w/v, solution), glucose, uric acid (UA) and ascorbic acid (AA) were received from Sinopharm Chemical Reagent Co. Ltd. (China). Carbon ink and silver chloride ink were bought from Yingman Nano Technology Jiangsu Co. Ltd. All solutions were prepared with deionized water.

The biosensor chips was produced with a 245 DEK (Weymouth, UK) screen-printing machine. The scanning electron microscopic (SEM) images and energy-dispersive X-ray (EDX) spectrum were examined using a field emission scanning electron microscope (FESEM) (Hitachi, ModelS-4800II, Japan). Transmission electron microscopy (TEM) experiments and Energy dispersive spectroscopic (EDS) analysis were performed with a JEOL JEM-2010 UHR. The enzyme solution was immobilized on the working electrode with NORDSON EFD (JR-V2303MI, Taiwan) three-dimensional dotting-enzyme machine. The glucose concentration in rabbit serum (Beijing Huaao Ke'an Technology Co. Ltd.) was analyzed by a glucometer (ACCU-CHEK@Performa Nano, Roche Diagnostics GmbH, Germany) to calibrate the results obtained by the as-prepared biosensor chips. The spectroscopy of carbon ink and PBNCs/AgNWs nanocomposites and PB and mixture were both investigated with Fourier-transform infrared (FTIR) (Thermo Electron, Nicolet-8700, and USA). The X-ray diffraction (XRD) of PB and AgNWs and carbon ink and mixture were measured on an X-ray diffractometer (D/MAX 2500 V/PC) with a Cu-Ka line (0.15419 nm). All of electrochemical measurements were executed in a 0.05 M phosphate buffered saline (PBS, pH = 6.5) containing 0.1 M KCl by using electrochemical workstation (CHI 660E, Shanghai Chenhua Instrument Co. Ltd. China). The ultrasonic cleaner (Kunshan Ultrasonic Apparatus Co. Ltd. China; volume: 4 L; power: 100 W; frequency: 40 KHz) was introduced to produce

more uniform dispersion of AgNWs. All no special temperature experiments were performed at room temperature.

2.2. Synthesis of AgNWs network

The two-step injection solution-based method is a typical synthesis of AgNWs (Hu et al. 2012). The 0.333 g of PVP was dissolved in 34 mL of EG with moderate stirring and heated to 160 ˚C until the temperature was stable in the three neck flask. Then 40 μL EG solution of NaCl (C_{NaCl} = 0.2 M) was added into the three neck flask, which was used to enhance the etched ability of the reaction solution on metallic silver and decrease the total generation rate of silver solids. It was one minute before 6 ml EG solution containing 0.34 g $AgNO_3$ (C_{AgNO3} = 0.333 M) was added into the three neck flask by using a syringe pump at a rate of 600 ul/min. When the phenomenon caused by the reaction solution was transformed nepheloid into limpid, all residual precursor solution was added into the three neck flask immediately. Then the three neck flask was sealed until the solution growing argenteous floccus, indicating the formation of AgNWs. The shape of AgNWs can be controlled by changing the concentration of $AgNO_3$ solution. The products were collected by centrifugation.

2.3. Synthesis of PBNCs /AgNWs nanocomposites

A facile method was used to fabricate PB, in which two precursor solutions of solution A: 5 mM $K_4[Fe(CN)_6]$ + 50 mM KCl + 100 mM HCl, and solution B: 5 mM $FeCl_3$ + 50 mM KCl + 100 mM HCl were prepared preliminarily. After solution A and solution B were poured into the syringe of 100 ml respectively, syringe was fixed on the injection pump. Afterwards, the ultrasonic cleaner was used to make 0.35 g AgNWs uniform dispersed in 50 mL distilled water and the 50 mL distilled water was added into the beaker as base solution, then the beaker as the reaction vessel into the heating magnetic stirrer stirred under the 35 ˚C. As shown in **Fig. 1**, once the solution

temperature in beaker was stable, the syringe with the speed of 500 μL/min was injected into the beaker. Specially, the drops of the two syringes must be consistent. The extent of the growth of PBNCs on the AgNWs can be controlled by controlling the synthetic time. Finally, we have successfully synthetized the most appropriate solution of PBNCs/AgNWs. The PBNCs/AgNWs nanocomposites were obtained by centrifuging PBNCs/AgNWs solution with the speed of 7000 rpm.

2.4. Preparation of mixture ink

The mixture ink was formed by mixing the PBNCs/AgNWs slurry with the carbon ink. Due to the screen-printing was highly required for the viscosity of the mixture ink. So the proportion of the PBNCs/AgNWs slurry and the carbon ink was constantly changed to achieve the most appropriate viscosity of mixture ink. Then a small quantity of ethanol was added into mixture ink. Furthermore， by constantly stirring the mixture ink, the PBNCs/AgNWs slurry and the carbon ink were uniformly blended. Specially, the mixture ink stopped stirring until the viscosity of the mixture ink can be printed.

2.5. The fabrication process of biosensor chips

The biosensor chip was produced with a 245 DEK (Weymouth, UK) screen-printing machine. A commercial polyethylene glycol terephthalate (PET) plate was served as the substrate for the screen-printing. The self-made mixture ink was used to prepare the working electrode (WE). Carbon ink was used to obtain the counter electrode (CE) and connector, and silver chloride was used to print the reference electrode (RE). We have been designed three shape of printing plate corresponding to three kinds of electrodes. The CE, RE and WE were printed in sequence through using corresponding printing plate.

2.6. Enzyme immobilization

In order to immobilize enzyme, the enzyme solution contained 0.25% glutaraldehyde (v/v), in which 1.8 U/μL GOx were included. Then, 4 μL of enzyme solutions were dotted evenly onto the center of the working electrode of biosensor chip with three-dimensional dotting-enzyme machine, followed by drying at the temperature of 4 ˚C.

3. Results and discussion

3.1. Growth of PBNCs on the AgNWs network

In order to build a 3D skeleton for the PB growth, the nanostructure and stacking morphology of AgNWs were well controlled. The width of each nanowire cannot be too narrow, otherwise a strong space limitation will hinder the regular crystallization of PB and obviously reduce the formative amount. In our previous works (Jiang et al. 2016), the normal size of PB crystal can be controlled about 100 nm. Accordingly, through the adjustment of synthesis concentration and time, the diameter of 200 nm AgNWs with an overlap style were built to provide a large surface area (Fig. 2A). In the absence of AgNWs, as shown in Fig. 2B, regular and uniform PBNCs were successfully synthesized to reach about the 100 nm size, and each crystal kept the independent distribution with rare aggregation. When the AgNWs were introduced during the PB preparation which followed the route of Fig. 1, the smooth surface of AgNWs was covered by the extremely small PB nanocrytals (Fig. 2C). The insert of Fig. 2E had evidently shown that PBNCs *in-situ* grew on AgNW. Different with the commonly used hydrothermal method (Carević et al. 2016), this growth and composite process was totally realized without any organic protective agent under the room temperature. In our design, the prepared PBNCs/AgNWs nanocomposite will be

served as the ink for the direct screen-printing of biosensors chip. Although the increasing amount of PB can be beneficial for the electrocatalysis enhancement, the over-deposition of PB will easily form a dense film to bury the network architecture, which causes the sudden reductions of both electrocatalysis and conductivity. Therefore, the morphology evolution of the prepared nanocomposite with the synthesis time is required to further investigate.

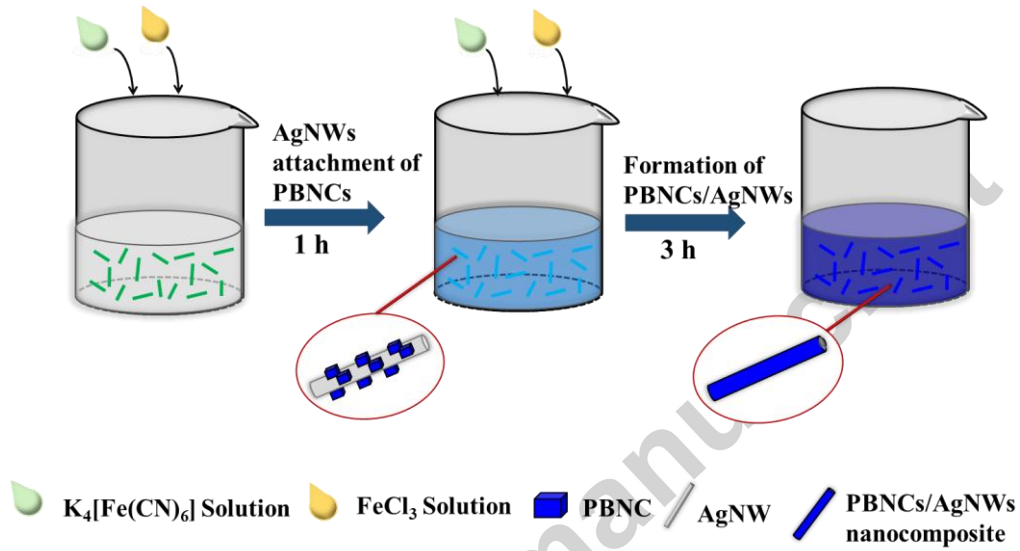

Fig. 1. Schematic illustration of the PBNCs/AgNWs nanocomposites fabrication process.

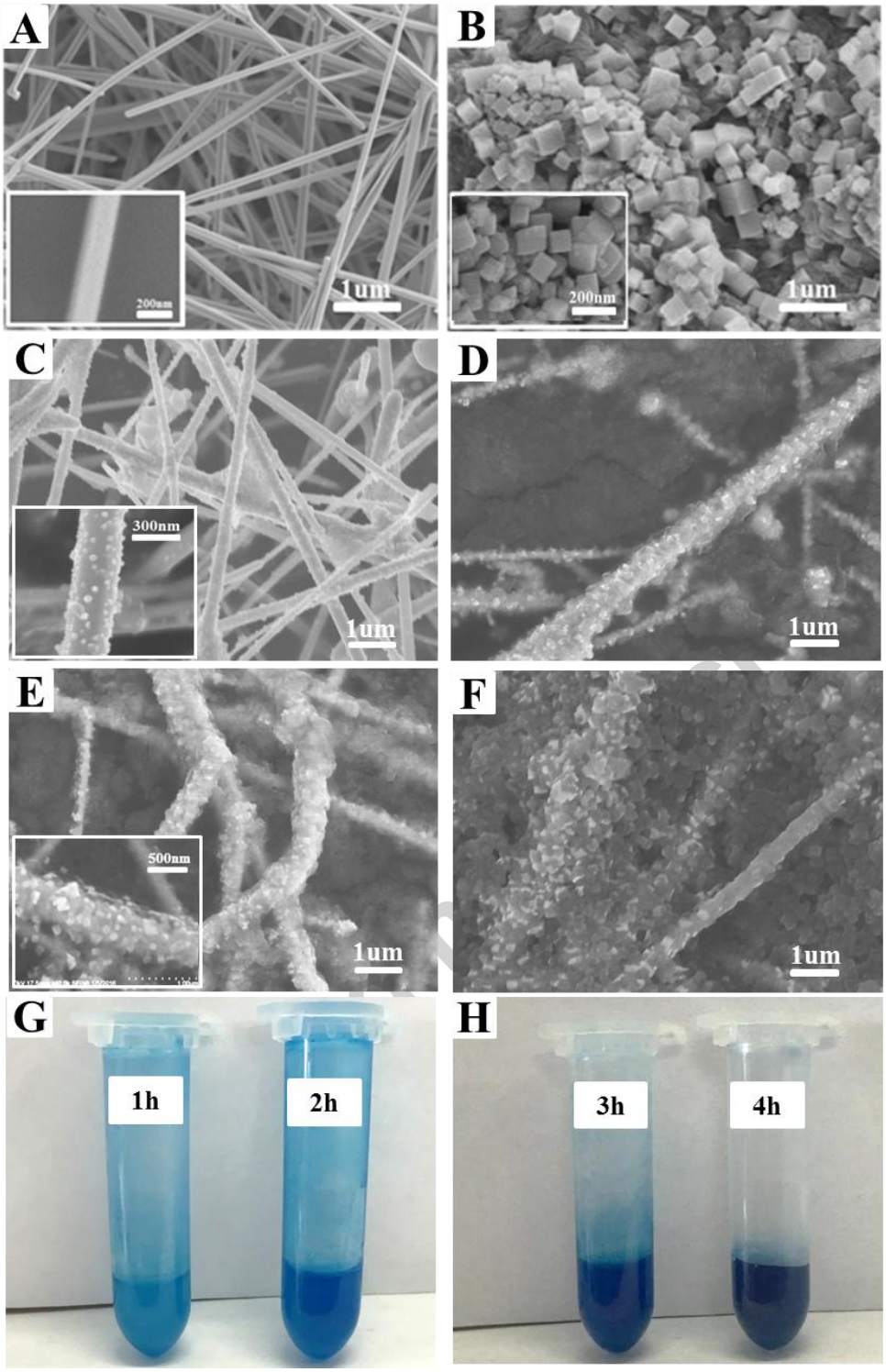

Fig. 2. FESEM images of (A) AgNWs network, (B) PBNCs and PBNCs synthesized with different growth time on 3D AgNWs network (C) 1 h, (D) 2 h, (E) 3 h and (F) 4 h, respectively. Photographs of (G) (H) were shown the production of colored changed with time. The inserts of (A) (B) (C) (E) were the magnified image of AgNWs and PBNCs.

The nanocomposite morphology and size distribution of the as synthesized samples can be seen from the corresponding SEM and TEM images in Figs. 2 and 3. As shown in Fig. 2, the nanocomposite inks prepared by different PB growth time from one to four hours were characterized to monitor the morphology evolution. Initially, only few of irregular PB nucleuses were synthesized on the partial sites of AgNWs, and most of AgNWs still kept the smooth surfaces (Fig.2C). With prolonging the growth time to 2 h (Fig. 2D), the bigger PB nanoparticles were formed on the 3D AgNWs network and covered almost surfaces of AgNWs, but the formation of PB nanoparticles was inhomogeneous on some AgNWs. Furthermore, the outline of nanoparticles was close to the cubic shape. Then, till the three hours, the thickness of PB layer increased obviously, and the well-defined PBNCs decorated the outside of the composite nanowires (Fig. 2E). However, when further improving the deposition time to 4 h, more and bigger PB crystals were aggregated to form a dense film which totally bury some of the AgNWs (Fig. 2F). In this case, the 3D structure of network was gradually replaced by a thick PB film, which cut down the function of AgNWs. Compared with the taken photos of above four inks (Fig. 2G and H), with the increase of the synthesis time of PB, the ink color will tend to the dark blue which indicates the increase of the ink viscosity. Furthermore, the as-prepared AgNWs and PBNCs/AgNWs nanocomposites were characterized by TEM to evaluate the structure and composition shown in Fig. 3. As shown in Fig. 3, the surfaces of AgNWs were very smooth with the diameter of ca. 203 nm. After the deposition of PB for 1 h, the diameter of nanocomposite wires obviously increased to ca. 532 nm (Fig. 3C). Moreover, the EDS result in Fig. 3D presented the new peaks of Fe and K elements which were attributed to the PB formation. With prolonging the growth time, the thickness of PB layer continuously increased, and the diameter of PBNCs/AgNWs

reached ca. 1μm (Fig. 3E). According to the comparison of Fig. 3D and 3E, it can be concluded that the further deposition can produce much more and bigger PB crystals which showed the high ratio of Fe/Ag elements.

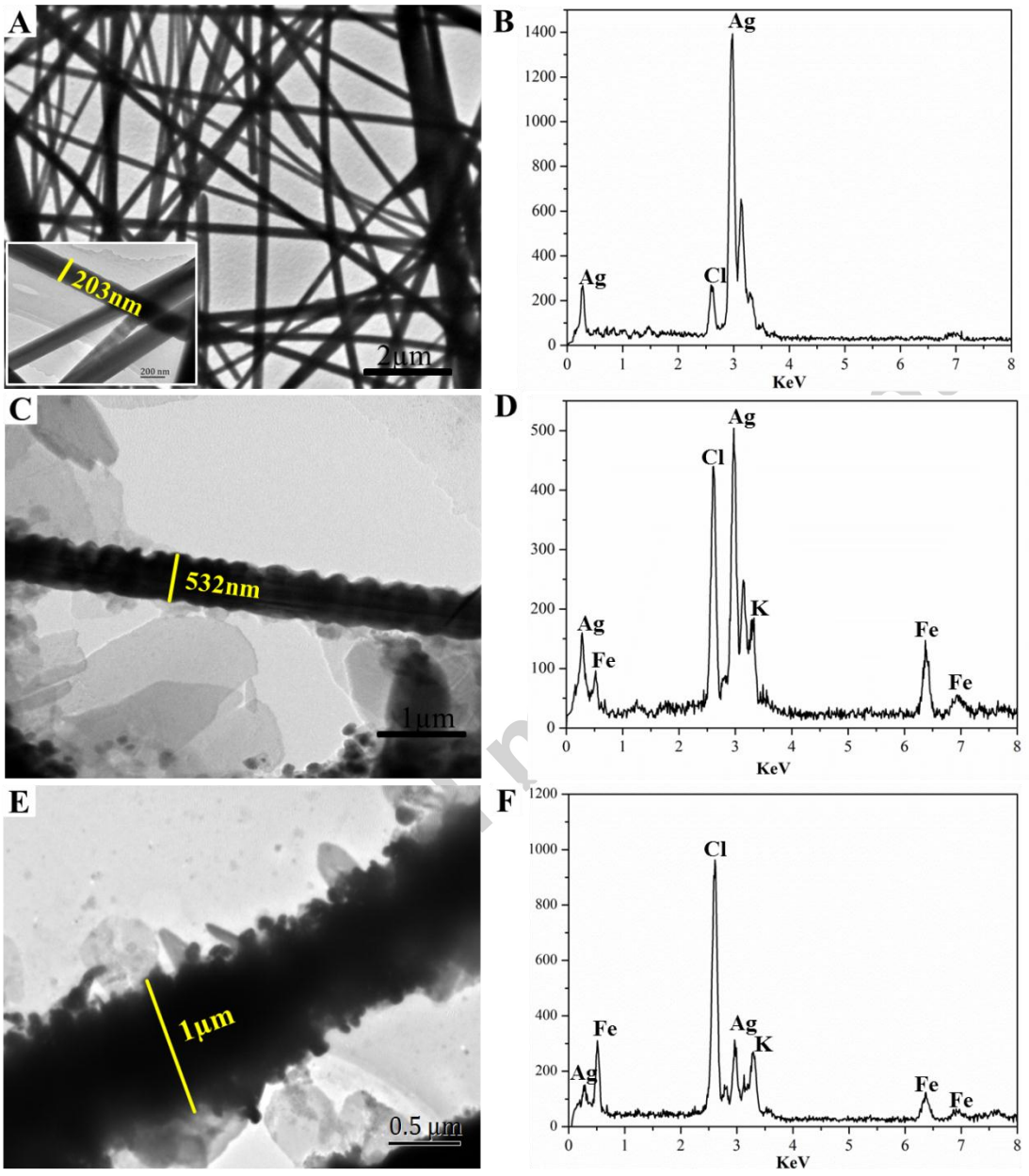

Fig. 3. TEM images of (A) the synthesized AgNWs network, (C) and (E) PBNCs/AgNWs networks prepared with different growth time 1 h and 2 h, respectively. (B), (D) and (F) EDS characterizations of samples in (A), (C) and (E), respectively.

The performance of PB has been confirmed to strongly affect by the nanostructure of the prepared film (Du et al. 2010). Therefore, the electrochemical redox properties

of PBNCs/AgNWs nanocomposites synthesized by different time were investigated (Fig. S1A). The redox mechanism of PB have expounded by Itaya et al in 1986 (Kingo et al. 1986). As shown in the following equation, PB and its reduced state Prussian white (PW) can reversibly and mutually convert under the cyclic voltammetry scanning.

$$Fe_4(III)[Fe(II)(CN)_6]_3 + 4e^- + 4K^+ \leftrightarrow K_4Fe_4(II)[Fe(II)(CN)_6]_3 \quad (2)$$

In the Fig. S1A, there was one couple of obvious redox peaks of ink, indicating the electron transfer behaviors of the PB reduction and PW oxidation. With the increase of PB growth time, both of the peak currents enhanced to present the increase of PB amount in the synthesized ink. However, the potential difference between reduction and oxidation peaks, which is determined by the resistance of electron transfer, were calculated as 0.113 V, 0.146 V, 0.163 V and 0.312 V for one to four hours synthesized nanocomposites. Above phenomenon was attributed to the low conductivity of PB crystals. Although the increase of the mass ratio of PB and AgNWs can obviously improve the electrocatalysis, the conductivity of the prepared ink will be greatly reduced due to the coverage of AgNWs surface to block the electron transfer through the body of each AgNW. In addition, glucose was selected to evaluate the performance of PBNCs/AgNWs nanocomposites. According to chronoamperometry results, the excellent linear relations of response currents vs glucose concentrations were exhibited in Fig. S2B. The sensitivities of the nanocomposites were calculated as 53.51, 77.96, 131.31, and 118.18 μA mM^{-1} cm^{-2} (the insert of Fig. S1) for the different growth time from one to four hours, respectively. According to above results, it was found that the highest sensitivity was obtained at the growth time of 3 h. Under this condition, the prepared nanocomposites can provide the enough amount of PB for the electrocatalysis. Meanwhile, the AgNWs cannot be buried by the excessive PB

crystals to fulfill the conductivity function. Hence, the PBNCs/AgNWs nanocomposites prepared at 3 h was selected as the optimum material for the ink preparation.

3.2. The fabrication of biosensor chips

In order to satisfy the viscosity requirement for screen-printing, the commercial carbon slurry was introduced to obtain the mixture ink which was formed by the mixture of the PBNCs/AgNWs nanocomposites and carbon slurry. Pure PBNCs, AgNWs, carbon ink, and mixture ink were characterized by the XRD patterns to investigate the structure stability of PB and Ag after the mixing operation. As shown in Fig. S2A, the six peaks located at 2θ = 17.69°, 25.00°, 35.56°, 39.89°, 51.12°, 54.36°, and 57.63° were assigned to the (200), (220), (400), (420), (440), (600), and (620) reflections of the PBNCs, respectively (Wu et al. 2006). Above result was consistent with the Joint Committee on Powder Diffraction Standards card (No. 73-0687) of standard PB crystal, indicating that the synthesized crystals were an integrated face-centered-cubic phase of PBNCs. The silver nanowires showed two peaks at 2θ = 38.0° and 44.3° which correspond to (1 1 1) and (2 0 0) of AgNWs, respectively (Coskun et al. 2011). When the PBNCs/AgNWs nanocomposites was mixed with carbon slurry to fabricate the screen-printing ink, the typical peaks of PBNCs, AgNWs and carbon ink were all retained to confirm the structure stability of PBNCs/AgNWs nanocomposite in the carbon slurry. Moreover, to ascertain the functional groups, the FTIR was further utilized to characterize the prepared screen-printing ink. As shown in Fig. S2B, the both of PBNCs/AgNWs

nanocomposites and mixture ink exhibited the strong absorption peak at 2090 cm^{-1} which belonged to the stretching absorption band of the -CN- group in the Fe^{2+}-CN-Fe^{3+} section of PB (Zhao et al. 2015), which demonstrated that the typical structure of PB can keep stable during the printing ink preparation. Compared with the PBNCs/AgNWs nanocomposites, the obviously exhibited band at around 1700 cm^{-1} of carbon slurry corresponded to the stretching vibration of the –COO−, confirming that abundant –COOH groups were formed. The present –COOH groups on the carbon slurry could facilitate the covalent immobilization of enzyme and further enhance the stability of the biosensor chips.

By using this nanocomposite ink, the working electrode was one-step screen-printed on a flexible polyethylene glycol terephthalate (PET) substrate, and the counter and reference electrodes were also printed to construct a miniature biosensor chip. It should be noticed that our prepared chip can possess the excellent flexibility (Fig. 4A) which can be beneficial for the storage and portability, and the curving behavior cannot produce the crack or peeling of the printed electrodes. Then the printing uniformity of working electrode was investigated by the EDX scanning. The characteristic elements, Fe in PBNCs and Ag in AgNWs, were respectively mapped and showed the uniform distribution in the working electrode (Fig. 4B). This result confirmed that the screen-printing process cannot produce the obvious aggregation of AgNWs and PBNCs in the partial locations of the working electrode, which was attributed to the strong combination by the *in-situ* growth of PBNCs on the AgNWs skeleton. The uniform distribution of the nanocomposites can be beneficial to

decrease the entire resistance of the working electrode, and improve the electron transfer rate.

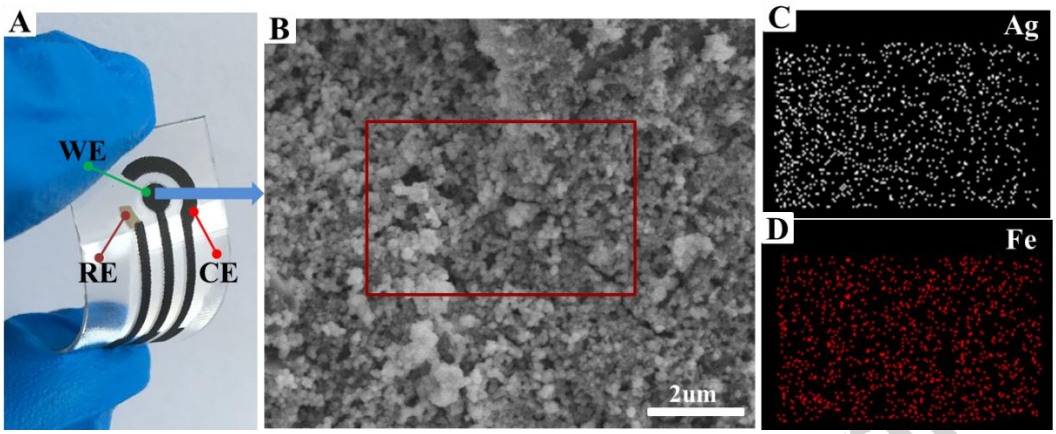

Fig. 4. (A) Digital image of the self-made flexible biosensor chip. (B) FESEM image of working electrode. EDX images of the selected region of working electrode, (C) silver element and (D) iron element.

3.3. Electrocatalytic performance of the as-prepared biosensor chips

PB possesses high electrocatalytic activity to the reduction of H_2O_2 due to the strong reduction ability, when PB is transformed to PW under the certain potential. Therefore, H_2O_2 can be served as the target to evaluate the electrocatalysis of PB. In Fig. 5A, the redox behaviors of the prepared biosensor chips were recorded by the CV scanning. After the addition of H_2O_2, the reduction peak current was increased, and the oxidation peak current was decreased. This phenomenon represents the reduction reaction of H_2O_2 by the PW transformed to PB as follow:

$$K_4Fe_4(\text{II})[Fe(\text{II})(CN)_6]_3 + 2H_2O_2 \rightarrow Fe_4(\text{III})[Fe(\text{II})(CN)_6]_3 + 4OH^- + 4K^+ \quad (3)$$

However, the function of AgNWs in the electrocatalytic process cannot be confirmed according to above result. Therefore, we fabricated two different chips which respectively applied PBNCs/AgNWs and only PBNCs as the inks for the screen-printed working electrodes for the investigation of the continuous electrocatalysis performance by the chronoamperometry experiment. The equivalent concentration of H_2O_2 was continuously injected at each of the same time interval. As shown in Fig. 5B, both chips can rapidly generate the steps of current after the each H_2O_2 addition, but the increasing rates of current for the same H_2O_2 concentration are quite different. Obviously, not only the value but also the stability of the current step produced by the PBNCs/AgNWs biosensor chip was higher than those of the PBNCs biosensor chip. We calibrated the linear relations between the response current and H_2O_2 concentration for the both chips (the inset of Fig. 5B). As calculation, the sensitivities of biosensor chips of PBNCs and PBNCs/AgNWs were 330.07 and 481.20 $\mu A\ mM^{-1}\ cm^{-2}$, respectively. It is obvious that the introduction of AgNWs can greatly increase the performance of chip by acceleration electrons transfer. This is probably due to the high conductivity and big contact area of AgNWs three-dimensional network. Because of the *in-situ* growth of PBNCs on the AgNWs skeleton, the size of PB nano-crystals was much smaller than the free grown crystals (Fig. 2). Therefore under the same preparation condition, the effective PB area was enhanced for the electrocatalysis. Moreover, all PBNCs were directly interacted on the wires, in this case, the electrons produced by the electrocatalytic reaction between PB and H_2O_2 can be fast transferred by the Ag skeleton to promote the reception of

current signal. Besides, the kinetic control mechanism of the as-prepared biosensor chips of PBNCs/AgNWs was investigated by the CV technology, which was continuously operated under different scanning rates. As shown in Figs. S3A and 3B, peak currents (I_{pc} and I_{pa}) linearly increased with the scan rate and achieved excellent correlation coefficients (0.9997 and 0.9994), indicating that the biosensor chips reaction is a surface controlled redox process (Samdani et al., 2016). Furthermore, with the increase of the scan rate (10 to 60 mV/s), ΔE_p was increased from 122 to 331 mV with nearly constant peak current ratio, suggesting that the electrochemical reaction of the biosensor chips corresponds to the quasi-reversible surface-controlled redox process (Wen et al., 2016).

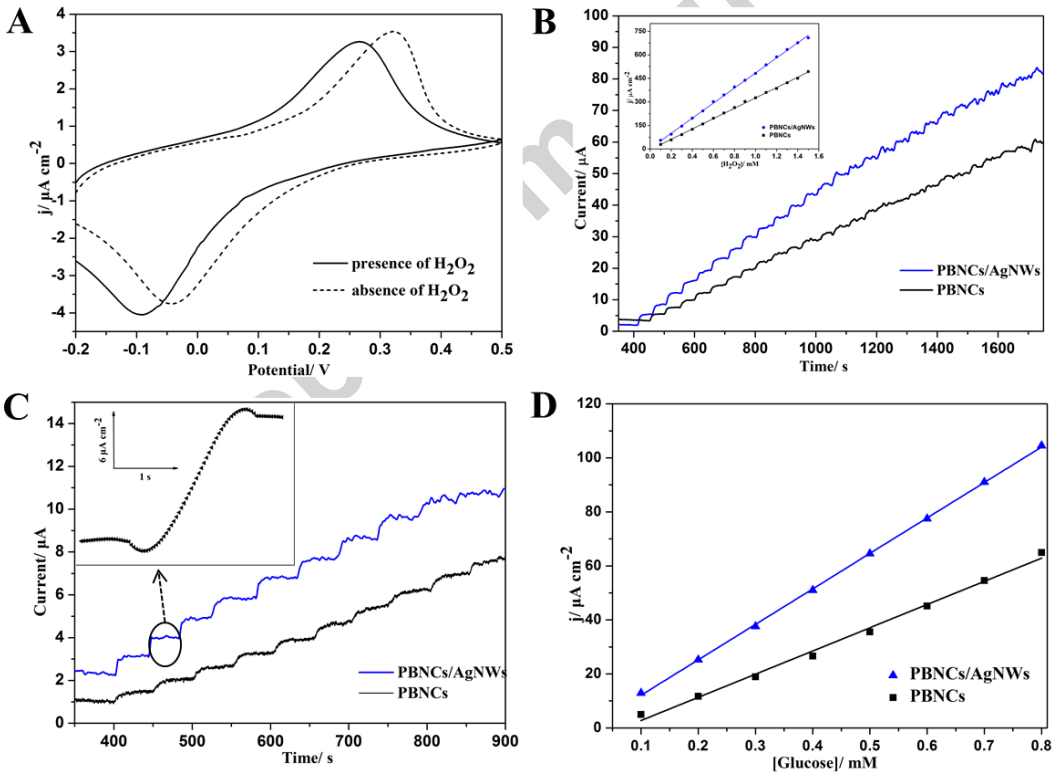

Fig. 5. (A) CV diagrams of the screen-printed chip with and without 1mM H_2O_2 in 0.05 M PBS solution at 25 ˚C, and the scan rate is 50 mV s^{-1}. Chronoamperometry curves of the screen-printed PBNCs/AgNWs and PBNCs based chips for the detection of (B) H_2O_2 and (C) glucose in 0.05 M

PBS solution at 25 ˚C. (D) Calibration curves of response current vs. glucose concentration according to the chronoamperometry results. The insert of (B) shows calibration curves of the corresponding chronoamperometry results. The insert of (C) showed the current response time after the addition of 0.1 mM glucose.

With the purpose of realizing the biosensing function, glucose oxidase was served as the sample enzyme to immobilize on the working electrode. By using the cross-linking method, the electrode surface was covered with the oxidase layer. Here, we also compared the electrocatalytic performance of PBNCs and PBNCs/AgNWs based biosensor chips in the detections of glucose. As shown in the chronoamperometry results (Fig. 5C), although the addition of 0.1 mM glucose can excite the step of current signal for both chips, the response period of PBNCs/AgNWs based chip was quite shorter with less than 3 s (the inset of Fig. 5C), which confirmed the promotion function of AgNWs to the transfer of electrons produced by the enzyme and PB reactions. According to the calculations (Fig. 5D), the sensitivities of the PBNCs and PBNCs/AgNWs based biosensor chips were 85.88 and 131.31μA mM^{-1} cm^{-2}, respectively. Also, the as-prepared biosensor chip based PBNCs/AgNWs exhibited a wider linear response from 0.01 mM to 1.3 mM with an ultralow LOD = 5 μM, and an excellent linear relation with R-Square = 99.97% for glucose. But the biosensor chips of PBNCs only have a linear response from 0.01 mM to 1.0 mM with an LOD = 10 μM, and an linear relation with R-Square = 99.38% for glucose. According to the above results, it can be proved that the introduction of AgNWs can

accelerate the electron transfer process and can increase the specific surface area of the PBNCs. In this electrocatalytic process, the glucose oxidase can fast generate the H_2O_2, and then the H_2O_2 will be reduced by PBNCs which possesses high electrocatalytic activity to produce the electrons. Under the each PBNC, numerous nanowires have been constructed a tight network to accelerate the electron transfer from PB to the substrate. We further compared the performance of the biosensor developed in this study with those of the various glucose biosensors reported in the literature. The table 1 can be divided into two categories: one was the PB modified biosensor; another was the other materials modified biosensor. The operation potentials of PB based biosensors were generally lower than 0 V, and the sensitivity of our prepared biosensor was higher than others listed in Table 1. This reason can be attributed to the synergic effect from the high electrocatalysis of PBNCs and the excellent conductivity of AgNWs. Although, some other materials (such as Platelet-like $Ni(OH)_2$ and $Ni(OH)_2/TiO_2$) based biosensors showed higher sensitivities, their operation potentials were generally higher than 0.5 V which may cause the simultaneous oxidation of the coexisting substances (UA and AA) to affect the detection accuracy in the practical analysis. All above results demonstrate that the 3D structured PBNCs/AgNWs nanocomposites can provide the synergic effects of high electrocatalysis and conductivity to the enzyme reaction of physiological substances under the very low potential.

Table 1 Performance comparison of the reported glucose biosensors.

Modifiers	Potential (V)	Sensitivity (mA M^{-1} cm^{-2})	LOD (μM)	ROD (mM)	Ref.
GOx/PBNCs/AgNWs	-0.05	131.31	5	0.01-1.3	This work
Au/PB/CS/CS-GOD	-0.1	82	0.397	0.002-0.4	(Wang et al. 2009)
GA/PB/graphite	-0.05	127.23	-	0.01-1.00	(Liu et al. 2014)
SPEs/PB/GA-Nafion-GOD	-0.05	63	1.0	0.002-0.1	(Ricci et al. 2003)
GOx/PB nancubes	-0.05	83.40	10	0.01-1.3	(Jiang et al. 2016)
GCE/PB/AuNPs-CS-GOD	-0.05	69.26	0.69	0.002-0.4	(Xue et al. 2006)
Pt/PB/GA-GOD	-0.05	80 ± 40	5.0	0.01-1.0	(Liu et al. 2009)
Platelet-like $Ni(OH)_2$	0.55	202	6.0	0.05-23	(Safavi et al. 2009)
AuNCs/graphene	-0.4	221	-	0.1-1.0	(Chu et al. 2015)
Ni-Ti-ONTs	0.6	83	0.13	2-200	(Hang et al. 2015)
$Ni(OH)_2/TiO_2$	0.5	192	8	0.03-14	(Gao et al. 2016)

3.4 Anti-interference ability, reproducibility and stability of the biosensor chips

The accuracy of biosensor is an essential parameter for the practical application, such as blood, fermentation solution and so on. As above mentioned, the real detection system often contains the complicated composition which can easily produce the interference signal due to the oxidation of the coexisted substances. Ascorbic acid (AA) and uric acid (UA) are the most common electrochemical interfering species because of their low oxidation potential in the blood or

fermentation systems. In order to investigate the anti-interference ability of the as-prepared biosensor chips, these two substances were successively added after the addition of glucose with the same concentration during the chronoamperometry testing. As shown in Fig. S5A, the current generated by the addition of glucose cannot show the obvious fluctuation after the addition of AA and UA. Because the operation potential (-0.05 V) of our chip is much lower than the oxidation potentials of AA and UA (0.2 V, 0 V) (Ma et al. 2014; Nakaminami et al. 1999)， which can avoid the other electrocatalytic reactions during the detection. Besides, there are many kinds of different sugars to be applied, such as maltose, sucrose, fructose, lactose, and mannose. Whether these similar structured sugars can also be electrocatalyzed to break the selectivity of the glucose biosensing? Hence, we also investigate the effects of above mentioned sugars on the detection of glucose. According to the results in Fig. S5B, we continuously added these sugars into the analytical system with the same concentration of glucose. However, no obvious current response was shown until the glucose was added. This result illustrated that the as-prepared biosensor chip can only work for the electrocatalysis of glucose due to the selectivity of the applied glucose oxidase. Meanwhile, the reproducibility of the fabricated biosensor chips was estimated by testing of twenty chips prepared in the different batches. The relative standard deviation (RSD) was 6.4%, in which indicated the designed biosensor chip possessed a satisfactory reproducibility. Besides, in order to investigate the stability, the chips were stored in the refrigerator at 4 ˚C for 30 days, and then examined their performance. The results showed that the steady-state response current retained about

75.47% of the initial sensitivity, which indicated that the considerably stability after storage.

3.5 Application of the biosensor chip in blood serum sample

In order to evaluate the accuracy of the biosensor chip in practical analysis (Shervedani, Amini and Sadeghi, 2016), the prepared biosensor chips were employed to measure concentration of glucose in rabbit blood serum. As shown in Fig. S4, 1 μL glucose (1 M) was first added into 10 ml PBS as the standard sample. Then 1 mL serum was added to test the current response. According to the calculation, the concentration of blood glucose tested by our prepared biosensor chip was 5.51 mM, and the glucometer detected level was 5.4 mM. Above comparison was repeated for four times, and the data were listed in the Table. S1. According to the results, the average deviation of detection in the rabbit serum was 3.08%, which demonstrated the accuracy of as-prepared biosensor chips were satisfactory.

4. Conclusions

In this work, we have successfully synthesized the PBNCs/AgNWs nanocomposites under the water environment. Well-defined 50 nm PBNCs were *in-situ* deposited on the skeleton of AgNWs to build a network structure. The nanocomposites were directly served as the screen-printing ink for the construction of a flexible biosensor chip. This chip has the both high electrocatalysis of PBNCs and fast conductivity of AgNWs to exhibit the synergic effects in the electrocatalytic detections of H_2O_2 and glucose under the very low potential, as well as has the

excellent anti-interference ability, reproducibility and stability. This synthesis route of nanocomposite ink can be extended in the preparation of more nanomaterials as the water-based inks for printing techniques, and the as-designed biosensor chip is promising in the large-scale production for the recognitions of various other physiological substances.

Acknowledgements

This work was supported by the Jiangsu Province Natural Science Foundation for the Youth (No. BK20140931), Top-notch Academic Programs Project of Jiangsu Higher Education Institutions (TAPP) and the Innovative Research Team Program by the Ministry of Education of China (No. IRT13070)

References

A. S. Rad, A. Mirabi, E. Binaian, T. Habibollah, 2011. International Journal of electronical science 6, 3671-3683.

Carević, M.V., Abazović, N.D., Novaković, T.B., Pavlović, V.B., Čomor, M.I., 2016. Applied Catalysis B: Environmental 195, 112-120.

Chu, Z., Liu, Y., Jin, W., Xu, N., Tieke, B., 2009. CHEM COMMUN(24), 3566.

Chu, Z., Liu, Y., Xu, Y., Shi, L., Peng, J., Jin, W., 2015. ELECTROCHIM ACTA 176, 162-171.

Chu, Z., Zhang, Y., Dong, X., Jin, W., Xu, N., Tieke, B., 2010. JOURNAL OF MATERIALS CHEMISTRY 20(36), 7815-7820.

Coskun, S., Aksoy, B., Unalan, H.E., 2011. CRYST GROWTH DES 11(11),

4963-4969.

Du, J., Wang, Y., Zhou, X., Xue, Z., Liu, X., Sun, K., Lu, X., 2010. The Journal of Physical Chemistry C 114(35), 14786-14793.

Espinoza-Castañeda, M., Escosura-Muñiz, A.D.L., Chamorro, A., Torres, C.D., Merkoçi, A., 2015. Biosensors and Bioelectronics 67, 107-114.

Gao, A., Zhang, X., Peng, X., Wu, H., Bai, L., Jin, W., Wu, G., Hang, R., Chu, P.K., 2016. Sensors and Actuators B: Chemical 232, 150-157.

Hang, R., Liu, Y., Gao, A., Bai, L., Huang, X., Zhang, X., Lin, N., Tang, B., Chu, P.K., 2015. Materials Science and Engineering: C 51, 37-42.

Hu, M., Gao, J., Dong, Y., Yang, S., Li, R.K.Y., 2012. RSC ADV 2(5), 2055.

Jiang, D., Chu, Z., Peng, J., Jin, W., 2016. Sensors and Actuators B: Chemical 228, 679-687.

Karyakin, A.A., Karyakina, E.E., 1999. Sensors and Actuators B: Chemical 57(1–3), 268-273.

Keihan, A.H., Sajjadi, S., 2013. ELECTROCHIM ACTA 113, 803-809.

Kingo, I., Isamu, U., VernonD, N., 1986. Accounts of Chemical Research 19(6), 162-168.

L. C. Clark, C.L., 1962. Ann. N. Y. Acad. Sci. 102, 29-45.

Liu, C., Sheng, Y., Sun, Y., Feng, J., Wang, S., Zhang, J., Xu, J., Jiang, D., 2015. Biosensors and Bioelectronics 70, 455-461.

Liu, L., Shi, L., Chu, Z., Peng, J., Jin, W., 2014. Sensors and Actuators B: Chemical 202, 820-826.

Liu, Y., Chu, Z., Jin, W., 2009. ELECTROCHEM COMMUN 11(2), 484-487.

Liu, Y., Chu, Z., Zhang, Y., Jin, W., 2009. ELECTROCHIM ACTA 54(28), 7490-7494.

Lu, J., Liu, S., Ge, S., Yan, M., Yu, J., Hu, X., 2012. Biosensors and Bioelectronics 33(1), 29-35.

Ma, Y., Zhao, M., Cai, B., Wang, W., Ye, Z., Huang, J., 2014. Biosensors and Bioelectronics 59, 384-388.

Nakaminami, T., Ito, S., Kuwabata, S., Yoneyama, H., 1999. ANAL CHEM 71(19), 4278-4283.

Piao, Y., Han, D.J., Azad, M.R., Park, M., Seo, T.S., 2015. Biosensors and Bioelectronics 65, 220-225.

Ren, C., Song, Y., Li, Z., Zhu, G., 2005. ANAL BIOANAL CHEM 381(6), 1179-1185.

Ricci, F., Amine, A., Palleschi, G., Moscone, D., 2003. Biosensors & Bioelectronics 18, 165-174.

Safavi, A., Maleki, N., Farjami, E., 2009. Biosensors and Bioelectronics 24(6), 1655-1660.

Samdani, K. J., Samdani, J. S., Kim, N. H., and Lee, J. H., 2016. Biosensors and Bioelectronics 81, 445-453.

Shervedani, R. K., Amini, A., and Sadeghi, N., 2016. Biosensors and Bioelectronics 77, 478-485.

Song, Y., Wang, L., Ren, C., Zhu, G., Li, Z., 2006. Sensors and Actuators B:

Chemical 114(2), 1001-1006.

Wang, H., Li, H., Zhang, Y., Wei, Q., Ma, H., Wu, D., Li, Y., Zhang, Y., Du, B., 2014. Biosensors and Bioelectronics 53, 305-309.

Wang, L., Ye, Y., Lu, X., Wu, Y., Sun, L., Tan, H., Xu, F., Song, Y., 2013. ELECTROCHIM ACTA 114, 223-232.

Wang, X., Gu, H., Yin, F., Tu, Y., 2009. Biosensors and Bioelectronics 24(5), 1527-1530.

Wen, Y., Wen, W., Zhang, X., and Wang, S., 2016. Biosensors and Bioelectronics 79, 894-900.

Wu, C., Sun, H., Li, Y., Liu, X., Du, X., Wang, X., Xu, P., 2015. Biosensors and Bioelectronics 66, 350-355.

Wu, X., Cao, M., Hu, C., He, X., 2006. CRYST GROWTH DES 6(1), 26-28.

Xu, Y., Chu, Z., Shi, L., Peng, J., Jin, W., 2015. Sensors and Actuators B: Chemical 221, 1009-1016.

Xue, M., Xu, Q., Zhou, M., Zhu, J., 2006. ELECTROCHEM COMMUN 8(9), 1468-1474.

Zhang, J., He, J., Xu, W., Gao, L., Guo, Y., Li, W., Yu, C., 2015. ELECTROCHIM ACTA 156, 45-52.

Zhang, Y., Sun, X., Zhu, L., Shen, H., Jia, N., 2011. ELECTROCHIM ACTA 56(3), 1239-1245.

Zhao, J., Liu, J., Tricard, S., Wang, L., Liang, Y., Cao, L., Fang, J., Shen, W., 2015. ELECTROCHIM ACTA 171, 121-127.

Highlights

- A three-dimensional PB nanocubes/Ag nanowires network was in-situ synthetized in the water.
- The network can be served as a water-based ink for the screen-printed flexible biosensor chip.
- The chips possess high sensitivity, selectivity and reproducibility under a very low potential.